Development 125, 3831-3842 (1998)
Printed in Great Britain © The Company of Biologists Limited 1998
DEV2298

Prx1 and *Prx2* in skeletogenesis: roles in the craniofacial region, inner ear and limbs

Derk ten Berge[1], Antje Brouwer[1], Jeroen Korving[1], James F. Martin[2] and Frits Meijlink[1,*]

[1]Hubrecht Laboratory, Netherlands Institute for Developmental Biology, Uppsalalaan 8, 3584 CT Utrecht, The Netherlands
[2]Alkek Institute of Biosciences and Technology, Center for Cancer Biology and Nutrition, Department of Medical Biochemistry and Genetics,Texas A&M University, Houston, Texas, 77030, USA
*Author for correspondence (e-mail: frits@niob.knaw.nl)

Accepted 14 July; published on WWW 7 September 1998

SUMMARY

***Prx1* and *Prx2* are closely related paired-class homeobox genes that are expressed in very similar patterns predominantly in mesenchyme. *Prx1* loss-of-function mutants show skeletal defects in skull, limbs and vertebral column (Martin, J. F., Bradley, A. and Olson, E. N. (1995) *Genes Dev.* 9, 1237-1249). We report here that mice in which *Prx2* is inactivated by a *lacZ* insertion had no skeletal defects, whereas *Prx1*/*Prx2* double mutants showed many novel abnormalities in addition to an aggravation of the *Prx1* single mutant phenotype. We found defects in external, middle and inner ear, reduction or loss of skull bones, a reduced and sometimes cleft mandible, and limb abnormalities including postaxial polydactyly and bent zeugopods. A single, or no incisor was present in the lower jaw, and ectopic expression of *Fgf8* and *Pax9* was found medially in the mandibular arch. A novel method to detect β-galactosidase activity in hydroxyethylmethacrylate sections allowed detailed analysis of *Prx2* expression in affected structures. Our results suggest a role for *Prx* genes in mediating epitheliomesenchymal interactions in inner ear and lower jaw. In addition, *Prx1* and *Prx2* are involved in interactions between perichondrium and chondrocytes that regulate their proliferation or differentiation in the bones of the zeugopods.**

Key words: Mouse, Homeobox gene, Gene targeting, aristaless domain, Epitheliomesenchymal interaction, Craniofacial development, Limb, Inner ear

INTRODUCTION

Vertebrate skeletal tissues arise from preskeletogenic condensations of mesenchymal cells. The central core of these condensations differentiates into cartilage or bone, while cells at the periphery form the perichondrium or periosteum. The superficial bones of face and skull form by intramembranous ossification. In contrast, most other bones are formed from cartilage elements by the process of endochondral ossification (see Erlebacher et al., 1995), in which a cartilaginous template is replaced by bone. Longitudinal growth then occurs by proliferating chondrocytes in the growth regions at both ends of the elements. Interactions with the perichondrium control the rate of proliferation and differentiation of the chondrocytes, and are important for correct bone morphogenesis (Vortkamp et al., 1996; Long and Linsenmayer, 1998).

Differentiation of mesenchymal precursor cells into defined skeletal elements is subject to local positional cues either by signals from nearby cells or from components of the adjacent extracellular matrix. In many cases, interactions between mesenchyme and neighbouring epithelia are required to initiate condensation. Transcription factors play an important role during early skeletal patterning, and it is likely that they operate in concert with signal factors and extracellular matrix molecules (Erlebacher et al., 1995; Hall and Miyake, 1995).

A subset of the vertebrate family of paired (prd)-class homeobox genes is characterised by the presence of a sequence encoding a conserved protein domain of unknown function near the carboxy terminus. Since this sequence is also found in the *Drosophila* transcription factor aristaless, which also contains a prd-class homeodomain, we termed it the aristaless domain. At least fourteen different vertebrate genes have been described that encode an aristaless domain, all of them also encoding a prd-class homeodomain (Ten Berge et al., 1998). The family of aristaless-domain-containing transcription factors differs also from paired and its vertebrate homologues (the Pax proteins) in that at position 50 of the homeodomain, which is important for its DNA-binding specificity, a lysine (Ptx) or glutamine (others) is present, instead of a serine. The *aristaless*-related genes thus form a group with distinct molecular characteristics. A subset of the *aristaless*-related genes is expressed mainly in mesoderm and neural crest-derived mesenchyme, and some of them have been shown to be involved in aspects of skeletogenesis. This subset includes the related genes *Prx1* and *Prx2* (formerly known as *MHox* and *S8*, respectively) which share extensive additional sequence

similarities (Cserjesi et al., 1992; Kern et al., 1992; Opstelten et al., 1991; this paper), and the likewise related genes *Alx3* (Rudnick et al., 1994; Ten Berge et al., 1998), *Alx4* (Qu et al., 1997a) and *Cart1* (Zhao et al., 1993).

The expression patterns of *Prx1* and *Prx2* show considerable overlap (Leussink et al., 1995). Mice homozygous for a *Prx1* null allele (Martin et al., 1995) show defects in skeletogenesis, including malformation of craniofacial, appendicular and axial structures. Most or all of the defects described were in tissues where both *Prx* genes are expressed, suggesting that *Prx2* was unable to compensate for the *Prx1* deficiency. We describe here the generation of mice carrying a *Prx2* gene inactivated by the in-frame insertion of a *lacZ* gene, using homologous recombination in ES cells. No defects could be found in mice homozygous for this mutation, whereas double mutants, generated by crossing the mice with the *Prx1* mutants described previously, showed many novel skeletal abnormalities, as well as an aggravation of the *Prx1* single mutant phenotype.

MATERIALS AND METHODS

Gene targeting

A genomic fragment carrying the last three exons of *Prx2* was isolated by screening a 129/Ola genomic library with a *Prx2* cDNA. A 1.8 kb PGK-Hygro fragment (Te Riele et al., 1990) was cloned into the *Bam*HI site of pSDKLacZ (gift of J. Rossant), a *lacZ*-Hygro cassette was isolated and, using *Not*I linkers, cloned into an *Eag*I site located 27 bp upstream from the *Prx2* homeobox (Figs 1A, 2A). The resulting construct pPrx2KO contained *lacZ* fused in-frame in the *Prx2*-coding sequence. *Sal*I-linearised pPrx2KO was electroporated into E14.IB10 ES cells, growing on SNLH9 feeders (Van Deursen and Wieringa, 1992). ES cell manipulations were generally as described by Wurst and Joyner (1993). Hygromycin-resistant clones were screened for *lacZ* activation upon a 48-hour treatment of 10^{-6} M retinoic acid, since this induces *Prx2* (De Jong and Meijlink, 1993). Southern analysis was then performed using the 5′ SR probe (Fig. 2A,B) and a 3′ cDNA probe (Fig. 2C). Chimeric mice were generated by both morula aggregation and blastocyst injection using B6D2F2 host embryos. Male chimeras were crossed to FVB and offspring carrying the mutation bred to homozygosity. Double mutants were obtained by crosses with *Prx1* heterozygous mutants (Martin et al., 1995). Genotyping was done by PCR on tail tip or yolk sac DNA. Four primer pairs were used that were capable of amplifying the *Prx2* wild-type allele (aggtgggtgagttagatggatagacc; gtgtgcgctcaaatacacgct; 340 bp product), the *lacZ* gene (gcatcgagctgggtaataagcgttggcaat; gacaccagaccaactggtaatggtagcgac; 821 bp product), the *Prx1* wild-type allele (ttcattccagatgaccagttgaact; ctggcctcagtgaggttcacc; 229 bp product), and the neomycin-resistance gene (actgggcacaacagacaatcg; cgtccagatcatcctgatcga; 410 bp product).

β-galactosidase staining

Whole-mount β-galactosidase staining of embryos was done as described (Hogan et al., 1994). Paraffin sections were cut at 7 μm and counterstained with neutral red. For embryos older than embryonic day 11 (E11) however, we noted increased difficulty in obtaining complete staining throughout the embryo. The alternative procedure, cryosectioning (see Hogan et al., 1994), suffers from poor histology and difficulty in obtaining complete series. A method to detect β-galactosidase activity in paraffin sections has been reported (Avé et al., 1997), but the sensitivity was low in our hands. We developed a sensitive method for demonstrating β-galactosidase activity in sections of tissue embedded in hydroxyethylmethacrylate polymer. The method combines the advantages of cryosections (high sensitivity) with those of plastic sections (complete series, high quality of histology). It has been tested successfully for mouse embryos ranging from E11.5 to E14.5, and is probably also applicable for later stages.

Embryos were fixed in 2% paraformaldehyde in PBS for 30 minutes (E11.5) to 2 hours (E14.5), followed by partial dehydration by graded ethanol series up to 90%, all on ice. They were infiltrated with 1:1 mixture of 90% ethanol/90% Technovit 8100 (T8100, Heraeus Kulzer GmbH, Wehrheim, Germany) for 1-2 hours, followed by 2 changes of 90% T8100 for 2 hours, all on ice. Embedding solution was prepared using 90% T8100 at room temperature, but otherwise according to the manufacturer's instructions. Prior to embedding, the embedding solution was allowed to polymerise for 5-10 minutes, until the solution was slightly viscous. The embedded embryos were cured overnight at room temperature and could conveniently be stored at 4°C for months without appreciable loss of β-galactosidase activity. When embedding and curing were done on ice, the β-galactosidase activity was lost in outer tissue layers. Sections were cut at 8 μm using glass knives and a Reichert-Jung 2050 motorised microtome, stretched on water and mounted onto slides. Slides were dried at 42°C overnight, stained in PBS containing 5 mM $K_3Fe(III)(CN)_6$, 5 mM $K_4Fe(II)(CN)_6$, 2 mM $MgCl_2$ and 1 mg/ml 5-bromo-4-chloro-3-indolyl-A-D-galactopyranoside (X-gal) at 37°C for 6-24 hours, counterstained by 0.1% aqueous neutral red or eosin for 30-60 seconds, rinsed with water, dried and coverslips mounted using DePex mounting medium (BDH, Poole, England).

Other histological techniques

To prepare sections from embryos and new-born mice the tissues were fixed overnight in PBS containing 4% paraformaldehyde. New-borns were decalcified in PBS containing 2.5% paraformaldehyde and 12.5% EDTA for 2 weeks, followed by an overnight rinse in running tap water. The tissue was then dehydrated, cleared and embedded in paraffin. Sections were cut at 7 μm and stained with haematoxylin and eosin. Bone and cartilage staining was done according to a modified procedure from C. Fromental-Ramain (IGBMC, Strasbourg). Foetuses and skinned and eviscerated new-born animals were fixed overnight in 96% ethanol, stained for cartilage in 80% ethanol, 20% acetic acid + 0.5 mg/ml alcian blue (Sigma) for 6-16 hours, rinsed 2 times in 96% ethanol for 3 hours and digested in 1.5% KOH for 2-6 hours, followed by bone staining in 0.5% KOH + 0.15 mg/ml alizarin red S (Sigma) overnight, destained in several changes of 20% glycerol + 1% KOH, transferred through a graded glycerol series and stored in 80% glycerol. Whole-mount and radioactive RNA in situ hybridisation was done as described (Leussink et al., 1995). *Bmp4*, *Fgf8*, *Pax9*, *Hoxd11*, and *Hoxd13* probes were kind gifts of B. L. M. Hogan (Nashville), G. R. Martin (San Francisco), R. Balling (Munich) and D. Duboule (Geneva), respectively.

RESULTS

Cloning of a complete *Prx2* cDNA

A 16.5-day mouse (NIH Swiss) embryo cDNA library in λEXLox (Novagen) was screened with a *Prx2* cDNA extending 44 bp upstream from the homeobox and a 5′ *Prx1* cDNA not containing the homeobox. Two clones contained inserts most likely covering the complete protein-coding region of *Prx2* (Fig. 1A). The putative start codon is in a favourable context (Kozak, 1987) and upstream from it in the same frame are two stop codons. Fig. 1B shows a comparison of the translation of the *Prx2* cDNA with that of the most similar of two splice variants of *Prx1* (Cserjesi et al., 1992). The high degree of similarity between the homeodomains and the part near the carboxy termini have been reported previously (Leussink et al., 1995; Cserjesi et al., 1992). *Prx1* and *Prx2*

share an N-terminal *Prx*-specific domain of 16 amino acids between positions 28 and 43 (Prx2) (Fig. 1A,B). This underscores the high degree of similarity between *Prx1* and *Prx2*, and presumably the related biochemical properties of the proteins encoded.

Generation of *Prx2* mutant mice

Mice lacking a functional *Prx2* gene were generated via homologous recombination in ES cells. Fig. 2 depicts the targeting strategy. The genomic organisation of part of the *Prx2* gene has been described previously (Opstelten et al., 1991). A *lacZ*/PGK-Hygromycin cassette was inserted into an *Eag*I site located upstream from the homeobox, such that the *lacZ*-encoding sequence is in-frame with the *Prx2*-coding sequence. Upon homologous recombination this allele is expected to express mRNA encoding the first 88 amino acids of the Prx2 protein fused to β-galactosidase protein, in a pattern identical to that of the *Prx2* gene. Due to the absence of both the homeodomain and the aristaless-domain it is unlikely that this protein retains any biochemical activity. Southern blotting using 5′ and 3′ probes (Fig. 2A) confirmed successful targeting in 18% of the hygromycin-resistant colonies (Fig. 2B,C). Two mouse lines carrying the mutant allele from independently derived ES clones were obtained.

Prx2$^{-/-}$ mice are viable and show no detectable abnormalities

Prx2$^{-/-}$ mutant mice were born at normal Mendelian ratios, and showed no obvious abnormalities. They developed into fertile and apparently healthy adults, with normal life span. The expression patterns of *Prx2* suggest a role in the development of the skeleton and of connective tissues like tendons (Opstelten et al., 1991; Leussink et al., 1995), and these aspects were studied further. Skeletons of new-born mice showed no abnormalities. Functional aspects of muscle/tendon complexes were tested in situ in a special measuring system (see De Haan et al., 1989). During isometric contractions, no difference was observed between control animals and *Prx2*$^{-/-}$ mutants in the length/power relations (elasticity) of the medial gastrocnemius muscle/tendon complex. Using dynamic contractions, no change was found in the interactions between tendons and muscles (A. de Haan, personal communication).

Absence of abnormalities in *Prx2*$^{-/-}$ mutants suggested that *Prx1* might compensate for loss of *Prx2*, as its sequence and expression pattern are very similar to those of *Prx2* (Fig. 1B; Leussink et al., 1995). *Prx1* null mutant mice show defects in skeletal elements of the head, the zeugopods of the limbs and the neural arches of the vertebrae (Martin et al., 1995), but

A

```
CGCCCCGACAAGGGGCGTGTGGCCCGGGCCGCTGGCTAGTGAGCGGTCCGCCCGTAGGGGAGGGCAGAAAGTTCGGGTCC 80
                                                                      M  D
CCGCACCGACTGACTTGAGATCCGGCACAGTGAGCAGCGGGAGGCGGCGGCGGCCGGCAGAGGCGCGGCCAGGGCATGGA 160
  S  A  A  A  A  F  A  L  D  P  P  A  P  G  P  G  P  P  P  A  P  G  D  C  A  Q
CAGCGCGGCCGCCGCCTTCGCCCTAGACCCGCCAGCGCCCGGCCCGGGGCCCCCGCCCGCACCCGGCGATTGCGCCCAGG 240
                 prx-domain
A  R  K  N  F  S  V  S  H  L  L  D  L  E  E  V  A  A  A  G  R  R  A  A  G  P  V
CGCGCAAGAACTTCTCGGTGAGCCACCTCCTGGACCTGGAGGAGGTGGCGGCTGCTGGGCGCAGGGCTGCGGGGCCCGTT 320
 S  G  P  A  E  A  R  V  G  A  A  R  E  P  S  G  G  S  S  G  T  E  A  A  P  Q  D
TCGGGGCCCGCCGAGGCGCGGGTGGGAGCGGCGCGCGAACCGTCCGGGGGCAGCAGCGGCACCGAGGCGGCGCCGCAGGA 400
  G  D  C  P  S  P  G  R  G  T  K  R  K  K  K  Q  R  R  N  R  T  T  F  N  S  S
CGGTGACTGTCCCAGCCCCGGCCGTGGCACCAAACGAAAGAAGAAGCAGCGCCGGAATCGAACCACATTCAACAGCAGCC 480
                 homeodomain
Q  L  Q  A  L  E  R  V  F  E  R  T  H  Y  P  D  A  F  V  R  E  E  L  A  R  R  V
AGCTGCAGGCGCTGGAGCGTGTATTTGAGCGCACACACTACCCTGACGCCTTTGTGCGTGAAGAGCTAGCTCGCCGTGTC 560
 N  L  S  E  A  R  V  Q  V  W  F  Q  N  R  R  A  K  F  R  R  N  E  R  A  M  L  A
AACCTCAGTGAGGCACGTGTCCAAGTCTGGTTCCAGAACCGCCGTGCCAAGTTTCGCCGGAATGAACGTGCCATGCTGGC 640
  T  R  S  A  S  L  L  K  S  Y  G  Q  E  A  A  I  E  Q  P  V  A  P  R  P  T  T
TACCCGCTCTGCCTCGTTGCTCAAGTCTTATGGCCAGGAGGCGGCCATTGAACAGCCTGTGGCCCCCCGACCTACCACGA 720
M  S  P  D  Y  L  S  W  P  A  S  S  P  Y  S  S  V  P  P  Y  S  P  G  G  S  S  P
TGAGCCCAGATTATCTATCCTGGCCAGCATCCTCCCCCTACAGCTCCGTGCCTCCCTATAGCCCCGGAGGTTCAAGTCCT 800
                 aristaless-domain
 A  T  P  G  V  N  M  A  N  S  I  A  S  L  R  L  K  A  K  E  F  S  L  H  H  S  Q
GCAACTCCTGGAGTCAACATGGCCAACAGCATCGCCAGCCTTCGCCTCAAGGCCAAAGAGTTCAGCCTACACCACAGCCA 880
  V  P  T  V  N  *
GGTGCCCACAGTGAACTGACTGTGCATTGGGTCCAGCTTCCTCCCTGGCCCAATGGCAGACTGCAGCAAAGGCAGTAGCC 960
TTGTCTGTCTCTGTCCTCAGACAAACTGGGCAGCCTCTCCCGTGCCTTTTCTCCATCACAGCTTCCTGAGTTCCAGAGGC 1040
CTGTTGGGTGCTGGAAGCAGTTGAACAAGTCACTGCTATGGTGGCTGAGATTGTGCCTAAGGCCCCTGGAGTGGCCTGGC 1120
CAGAAGGCGGAGCTGGAGTCCGCCAAGGAACTCACTTACTTATGTATTAAAACCAAAAAGCTTTTGTCTTTAAGGAATAA 1200
AACCATTTTTCGTAAGCTCAA 1221
```

B

```
                                                prx-domain
      * *    +   +*   *    *   *  **+*************          *   *+  *
Prx1  MTSSYGHVLERQPALGGRLDSPGNLDTLQAKKNFSVSHLLDLEEAGDM-------VAAQADESV  57
Prx2  MDSA-AAAFALDPPAPGPGPPPAPGDCAQARKNFSVSHLLDLEEVAAAGRRAAGPVSGPAEARV  63

                                                homeodomain
      * *     *  * +**++   ** *        *+*+*****************************
Prx1  GEAGRSLLESPGLTSGSDTPQQDND--QLNSEEKKKRKQRRNRTTFNSSQLQALERVFERTHYP 119
Prx2  GAAR----EPSGGSSGTEAAPQDGDCPSPGRGTKRKKKQRRNRTTFNSSQLQALERVFERTHYP 123

      ******+*******+************************ + *******  +  *+***++***
Prx1  DAFVREDLARRVNLTEARVQVWFQNRRAKFRRNERAMLANKNASLLKSYSGDVTAVEQPIVPRP 183
Prx2  DAFVREELARRVNLSEARVQVWFQNRRAKFRRNERAMLATRSASLLKSYGQE-AAIEQPVAPRP 186

                                                aristaless-domain
          +*****   ****    **          *+******* *******+**   ******
Prx1  APRPTDYLSWGTASPYSAMATYSATCANNSPAQGINMANSIANLRLKAKEYSLQRNQVPTVN   246
Prx2  TTMSPDYLSWPASSPYSSVPPYSPG-GSSPATPGVNMANSIASLRLKAKEFSLHHSQVPTVN   248
```

Fig. 1. The *Prx2* mRNA and protein. (A) Nucleotide and predicted amino acid sequence of *Prx2* cDNA and protein. Two stop codons upstream and in frame with the putative translation initiation codon are underlined. The three conserved protein domains (homeodomain, aristaless domain and *Prx*-specific domain) and the nucleotide sequences encoding them are shaded. Accession numbers X52875; S57868. (B) Comparison of Prx1 and Prx2 proteins. Conserved domains are shaded, identical amino acids are marked with an asterisk and conservative changes with a plus sign.

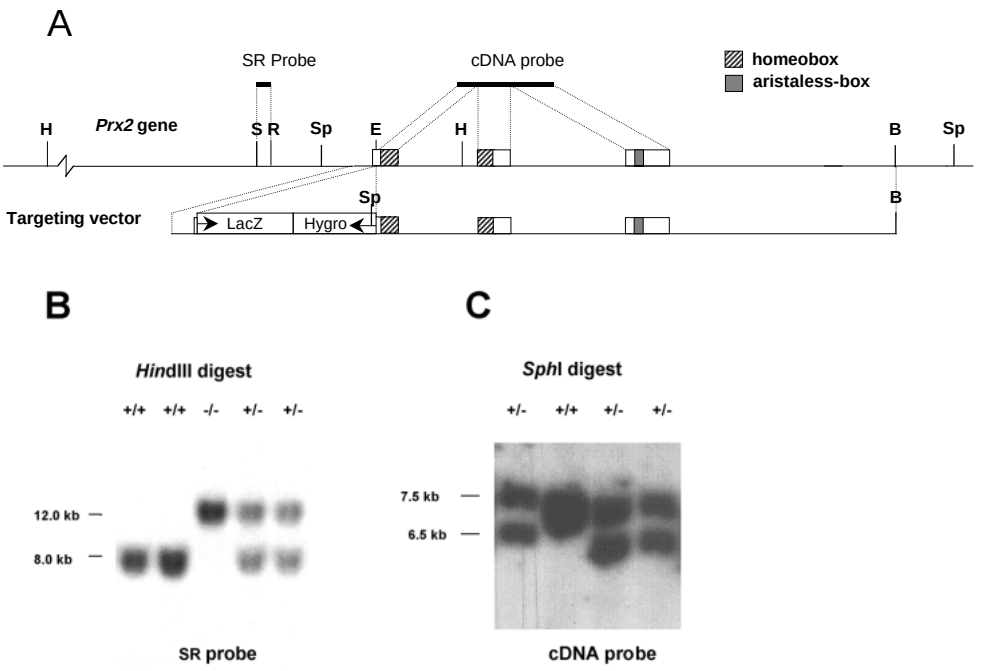

Fig. 2. Targeted mutagenesis of *Prx2*, and genotype analysis of mice and ES cells. (A) The diagram illustrates the structure of the *Prx2* locus (top) and the targeting vector (below). The last three exons of the *Prx2* gene are depicted by rectangles. The homeobox and the aristaless-box (encoding the aristaless-domain) are shaded. A 5 kb *lacZ*/PGK-Hygro cassette (not to scale) was inserted just upstream from the homeobox. Arrows indicate direction of transcription. Relevant restriction sites and probes are indicated. The SR probe is located outside the modified region, the cDNA probe is a partial cDNA detecting only exon sequences downstream from the insertion site of the *lacZ*/PGK-Hygro cassette. B, *Bam*HI, E, *Eag*I, H, *Hin*dIII, R, *Eco*RI, S, *Sst*I, Sp, *Sph*I. (B) Example of genotyping mice by DNA blot hybridisation of *Hin*dIII-digested DNA using the SR probe. The wild-type allele is detected as a 7 kb fragment, the targeted allele as a 12 kb fragment due to the insertion of the cassette. +/+, +/– and –/– indicate wild-type, heterozygous and homozygous mutant animals, respectively. (C) Example of genotyping ES cells by DNA blot hybridisation of *Sph*I-digested DNA using the cDNA probe. The mutant allele has an *Sph*I fragment of 6.5 kb versus 7.5 kb of the wild-type allele, due to the presence of an *Sph*I site in the PGK promoter.

other structures in which both *Prx1* and *Prx2* are expressed, such as other parts of the limbs, jaws and otic capsule, develop normally. Therefore we crossed both mutants to generate double mutant mice.

Prx1$^{-/-}$*Prx2*$^{-/-}$ double mutant mice show many abnormalities not found in either single mutant

Prx1$^{-/-}$*Prx2*$^{-/-}$ double mutant mice died within an hour after birth, while *Prx1*$^{-/-}$ single mutants lived for up to 24 hours. The double mutants showed a severely reduced lower jaw (micrognathia), a pointed snout, absence of external ears (anotia) and downward pointing forelimbs (Fig. 3A-C). Approximately 8 percent of the new-borns showed a cleft mandible and tongue (Fig. 3D; Table 1). The animals appeared cyanotic, indicating a lack of oxygen. *Prx1*$^{-/-}$ as well as *Prx1*$^{-/-}$*Prx2*$^{-/-}$ mutants displayed a cleft secondary palate (Martin et al., 1995; Fig. 3F,G). In *Prx1*$^{-/-}$*Prx2*$^{-/-}$ mutants, presumably as a consequence of the reduced lower jaw, the tongue inserted through the cleft palate into the nasal cavity, probably obstructing the airways (Fig. 3G). This may have caused the rapid death of these mutants.

New-born mortality was also observed in *Prx1*$^{+/-}$*Prx2*$^{-/-}$ mutant mice, although neither *Prx1*$^{+/-}$ mice nor *Prx2*$^{-/-}$ mice displayed abnormalities. Initially about 80% of *Prx1*$^{+/-}$*Prx2*$^{-/-}$ new-borns showed respiratory problems and abdominal distension because of cleft secondary palate, and died within 24 hours. Those that survived reached adulthood and displayed no health problems. From their offspring, most *Prx1*$^{+/-}$*Prx2*$^{-/-}$ new-borns survived without problems, indicating that lethality depended on genetic background.

Skeletal abnormalities in the lower jaw

The *Prx1*$^{-/-}$*Prx2*$^{-/-}$ mutant phenotype was studied by analysis of sections and skeletal stains of new-borns and embryos. New-borns showed a striking reduction of the lower jaw (Fig. 3C). The dentaries were shortened, and their distal tips fused (Fig. 4F). Most of Meckel's cartilage was deleted, only the distal tip and a small proximal part including a malformed malleus being present, and an ectopic process was visible immediately distal from the malleus (Fig. 5E). The malleus and ectopic process were similarly affected as described previously for *Prx1*$^{-/-}$ mutants (Martin et al., 1995; Fig. 5C). The mandibular incisors were either absent (Fig. 4F), or a single median incisor was found (Fig. 4E), whereas the molars were unaffected (Fig. 3G). In some cases, a fragment of a second incisor was found. Specimens with cleft mandible showed remnants of an incisor on both dentaries (Fig. 4D). Table 1 shows the occurrence of aspects of the phenotype with incomplete penetrance.

Prx1$^{-/-}$*Prx2*$^{+/-}$ new-borns had shortened dentaries and closely spaced incisors, and demonstrated a phenotype intermediate between those found in *Prx1*$^{-/-}$ and *Prx1*$^{-/-}$*Prx2*$^{-/-}$ mutants (Fig. 4C). The correlation between progressive loss of *Prx* function and medial shift of the incisors suggests a role for *Prx* genes in specification of mandibular midline structures.

Table 1. Frequency of partially penetrant defects in *Prx1*$^{-/-}$*Prx2*$^{-/-}$ mutant mice

Structure	Defect	Frequency (%)
Mandible (*n*=26)	Incisors absent	38
	Single incisor	42
	Partial second incisor	12
	Cleft mandible	8
Forefoot (*n*=15)	Ectopic metacarpal + phalanges	20
	Ectopic metacarpal fragment	80
Scapula (*n*=26)	Absence of spine	62

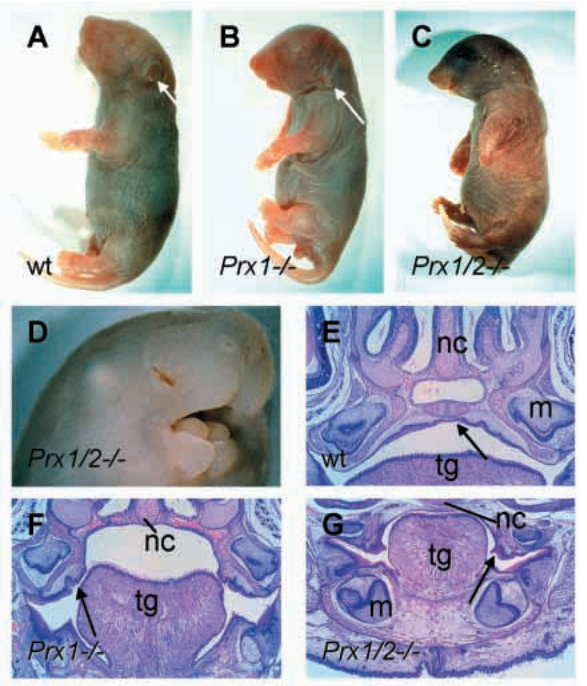

Fig. 3. Lateral views of (A) wild-type, (B) *Prx1*$^{-/-}$ and (C) *Prx1*$^{-/-}$ *Prx2*$^{-/-}$ new-born mice. Note micrognathia and anotia in C, and downward pointing limbs in B and C. (D) Cleft mandible in E18.5 *Prx1*$^{-/-}$*Prx2*$^{-/-}$ foetus. (E-G) Frontal sections through the oral cavity of (D) wild-type, (E) *Prx1*$^{-/-}$ and (F) *Prx1*$^{-/-}$*Prx2*$^{-/-}$newborn mice. Arrows indicate the ears in A,B, the secondary palate in E, and the palatal processes in F and G. The oral cavity in G cannot accommodate the tongue, which therefore obstructs the airway. Abbreviations: m, molar; nc, nasal cartilage; tg, tongue.

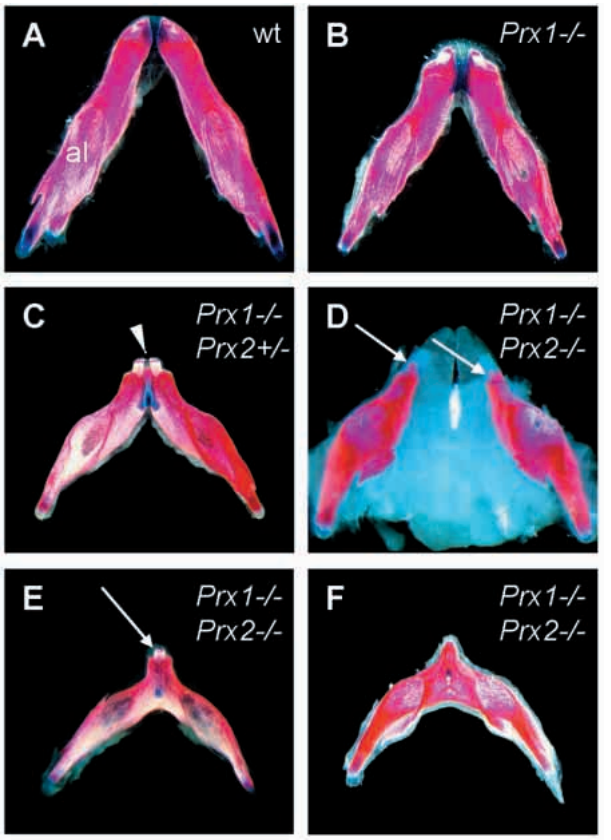

Fig. 4. Dissected mandibles from (A) wild-type, (B) *Prx1*$^{-/-}$, (C) *Prx1*$^{-/-}$*Prx2*$^{+/-}$ and (D-F) *Prx1*$^{-/-}$*Prx2*$^{-/-}$ mutant new-borns. (D) Cleft of mandibular bone and soft tissue. Arrows in D indicate remnants of the incisors. Note the reduced distance between the incisors in C (arrowhead), the single incisor in E (arrow) and absence of the incisors in F. Abbreviation: al, alveolar process.

To get further insight into the role of *Prx2*, its expression during development of the lower jaw was visualised by β-galactosidase staining in *Prx2*$^{+/-}$ embryos (Fig. 6). Comparison with the results of radioactive in situ hybridisation (Leussink et al., 1995) confirmed that β-galactosidase staining faithfully represented *Prx2* expression. The expression patterns were essentially the same in *Prx2*$^{+/-}$ mutants as in *Prx1*$^{-/-}$ *Prx2*$^{-/-}$ mutants, indicating that the *Prx* genes exert no cross or autoregulation. From embryonic day 8.5 (E8.5) to E10.5, high expression was found in the mesenchyme of the distal part of the mandibular arch (shown for E9.5 in Fig. 6C,E). At E11.5, two epithelial thickenings, called dental epithelium, form the first morphological signs of incisor development, and β-galactosidase expression was restricted to the mesenchyme of the distal-medial part of the mandibular arch, including the area underneath the dental epithelium (not shown). At E12.5, when the incisor buds form, expression was found medially in the distal part of the mandible underneath the incisor buds and surrounding the mesenchymal condensations of the distal tip of Meckel's cartilage (Fig. 6A). Expression more proximal in the lower jaw was weaker and concentrated underneath the dental lamina, in a domain abutting Meckel's cartilage dorsally, and laterally from Meckel's cartilage in condensed mesenchyme, presumably the progenitor of the dentary (Fig. 6B). *Prx1* was expressed similarly at E12.5 as determined by radioactive in situ hybridisation (not shown).

Development of the mandibular arch in *Prx1*$^{-/-}$*Prx2*$^{-/-}$ mutant embryos appeared normal up to E10.5. At E11.5, a large area of thickened epithelium was found, spanning the distal-medial region of the mandibular arch, instead of the two dental epithelial thickenings normally present (not shown). At E12.5, this thickened epithelium was still present and no incisor bud was formed (Fig. 6D). The mesenchymal condensations for Meckel's cartilage were absent (Fig. 6D), except in the proximal part and the tip of the mandible, and the lower jaw was much shorter than normal (not shown). In sections of E13.5 *Prx1*$^{-/-}$*Prx2*$^{-/-}$ embryos, a single medial incisor bud of normal morphology was present (not shown; *n*=2). Skeletal stains revealed that only the proximal part of Meckel's cartilage and a cartilaginous sphere at the tip had formed in E13.5 and E14.5 *Prx1*$^{-/-}$*Prx2*$^{-/-}$ mutants (Fig. 7D). Meckel's cartilage was completely present in *Prx1*$^{-/-}$ mutants, but only partially in *Prx1*$^{-/-}$*Prx2*$^{+/-}$ mutants (compare Fig. 7B,C).

The signalling factors Bmp4 and Fgf8 and the transcription factor Pax9 have been implicated in positioning the incisors. Antagonistic interactions between epithelially expressed *Fgf8* and *Bmp2/4* regulate *Pax9* in the underlying mesenchyme, a marker of presumptive tooth mesenchyme (Neubüser et al., 1997). At E10.5, the expression domain of *Fgf8* in the *Prx1*$^{-/-}$ *Prx2*$^{-/-}$ mutant showed a faint ectopic extension running medially along the mandibular process (not shown). At E11.0,

the domain of *Fgf8* expression had shifted laterally, while an extension of the domain showing low expression was running medially (compare Fig. 8A,B). The domain of *Bmp4* expression no longer overlapped with *Fgf8* expression (compare Fig. 8C,D). *Pax9* was expressed in the mesenchyme underneath the ectopic medial domain of *Fgf8* expression (compare Fig. 8E,F). At E11.5 *Fgf8* was no longer expressed in wild-type or *Prx1*$^{-/-}$*Prx2*$^{-/-}$ mandibular arch. *Pax9* expression in the wild type was found in two lateral presumptive molar domains and in two presumptive incisor domains more medially located, while a single medial domain was present in the *Prx1*$^{-/-}$*Prx2*$^{-/-}$ mutant (Fig. 8G,H). The single medial domain of *Pax9* expression correlates well with the observation of a medial incisor.

Abnormalities in the second pharyngeal arch

Reichert's cartilage is the skeletal element associated with the second pharyngeal arch. In mammals, Reichert's cartilage gives rise to the greater part of the stapes and to the lesser horn (and part of the body) of the hyoid bone, the styloid process and the stylohyoid ligament, which connects the lesser horn to the styloid process. The stylohyoid ligament was not formed completely in the *Prx1*$^{-/-}$ mutant, and part of it developed as a cartilaginous element (Martin et al., 1995; Fig. 5D). In contrast, in *Prx1*$^{-/-}$ *Prx2*$^{-/-}$ mutants, the entire stylohyoid ligament chondrified, and connected the stapes (not shown) and styloid process to the lesser horn of the hyoid bone (Fig. 5F). The site of attachment of the stapes to the otic capsule, called the oval window, was displaced medially (not shown). This may be secondary to the displacement of the stapes, as the stapedial blastema induces formation of the oval window. The chondrified stylohyoid ligament was also found in *Prx1*$^{+/-}$*Prx2*$^{-/-}$ mice. This, and the cleft secondary palate, were the only abnormalities found in these mice (data not shown). *Prx2* expression was found from E9.5 to E11.5 in the region near the otocyst where the future ossicles will develop (not shown). From there a rod of expressing cells was seen, running down from the otic region parallel to the branchial artery towards the distal tip of the second arch (shown for E9.5 in Fig. 6C,E). At E12.5, only very faint β-galactosidase expression was visible in the second arch (not shown). These observations suggest that *Prx2* may be expressed in second arch mesenchyme destined to form Reichert's cartilage, and is required to drive differentiation towards ligament instead of cartilage. High expression was also visible in the endoderm of the second and third pharyngeal pouch, and in the ectoderm of the corresponding grooves from E9.5 to E11.5 (Fig. 6C,E). It is possible that correct formation of Reichert's cartilage requires signals from the pharyngeal pouch endoderm and *Prx2* may regulate such signals.

Abnormal development of semicircular ducts

The mammalian inner ear develops from a spherical epithelial vesicle, the otocyst. By a series of complex shape changes the otocyst produces a number of sensory structures, namely the cochlea, containing the auditory apparatus, the saccule and utricle, containing sensors of linear acceleration, and the three semicircular ducts, containing sensors of angular acceleration. Saccule, utricle and semicircular ducts are collectively termed the vestibule, and vestibule and cochlea together form the membranous labyrinth. During embryogenesis, the mesenchyme surrounding the membranous labyrinth chondrifies and forms the otic capsule, and the semicircular ducts run through spaces in the capsule called semicircular canals.

Mutation of *Prx1* and *Prx2* resulted in a reduced size of the entire otic capsule and absence of the lateral semicircular canal

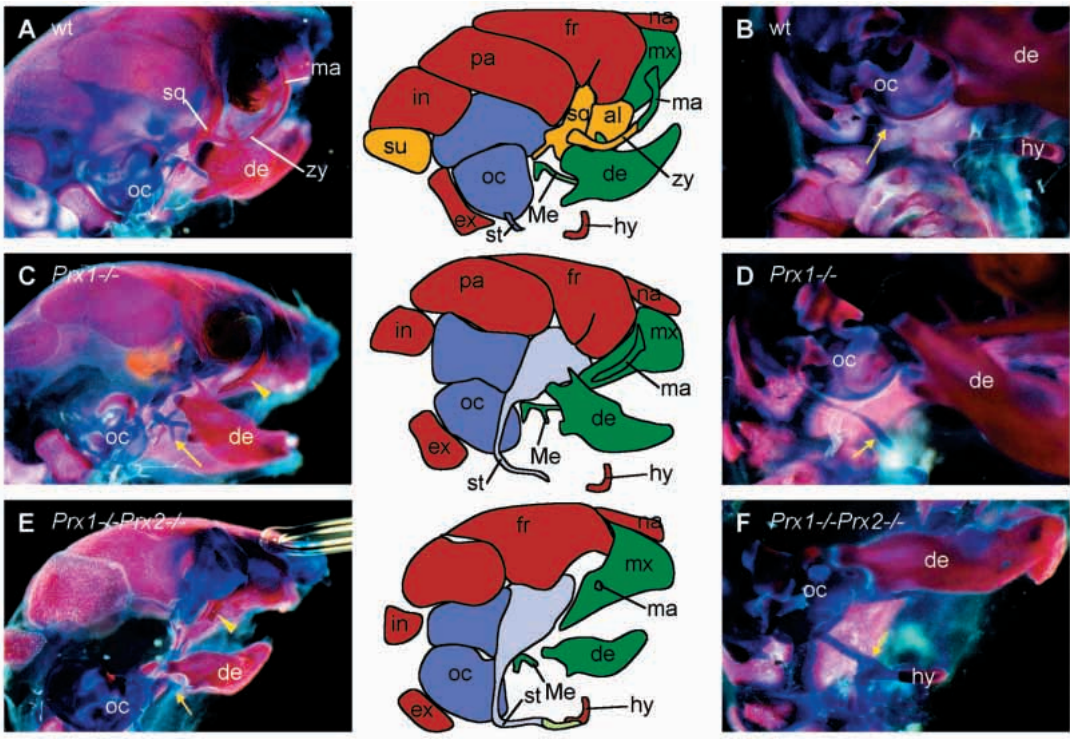

Fig. 5. Skeletal abnormalities in skull of *Prx1/2* mutant mice. Skeletal stains of (A,B) wild-type, (C,D) *Prx1*$^{-/-}$ and (E,F) *Prx1*$^{-/-}$*Prx2*$^{-/-}$ new-born mice with corresponding diagrams. An abnormal process is visible on Meckel's cartilage of *Prx1*$^{-/-}$ and *Prx1*$^{-/-}$*Prx2*$^{-/-}$ mutants (arrows in C,E). The malar process of the maxillary bone (arrowhead in C, green in diagram) is absent in *Prx1*$^{-/-}$*Prx2*$^{-/-}$ mutant (arrowhead in E). Arrows in B,D,F indicate styloid process, which is elongated in *Prx1*$^{-/-}$ mutants (D, light blue in diagram), and fused to the hyoid bone in *Prx1*$^{-/-}$*Prx2*$^{-/-}$ mutants (F). Diagram colours: red, bone; blue, cartilage; light blue, ectopic cartilage in *Prx1*$^{-/-}$; light green, ectopic cartilage in *Prx1*$^{-/-}$*Prx2*$^{-/-}$; yellow, reduced/deleted in *Prx1*$^{-/-}$; green, reduced in *Prx1*$^{-/-}$*Prx2*$^{-/-}$. Abbreviations: al, alisphenoid; de, dentary; ex, exoccipital; fr, frontal bone; hy, hyoid bone; in, interparietal bone; ma, malar process; Me, Meckel's cartilage; mx, maxillary; na, nasal bone; oc, otic capsule; pa, parietal bone; sq, squamosal; st, styloid; su, supraoccipital; zy, zygomatic.

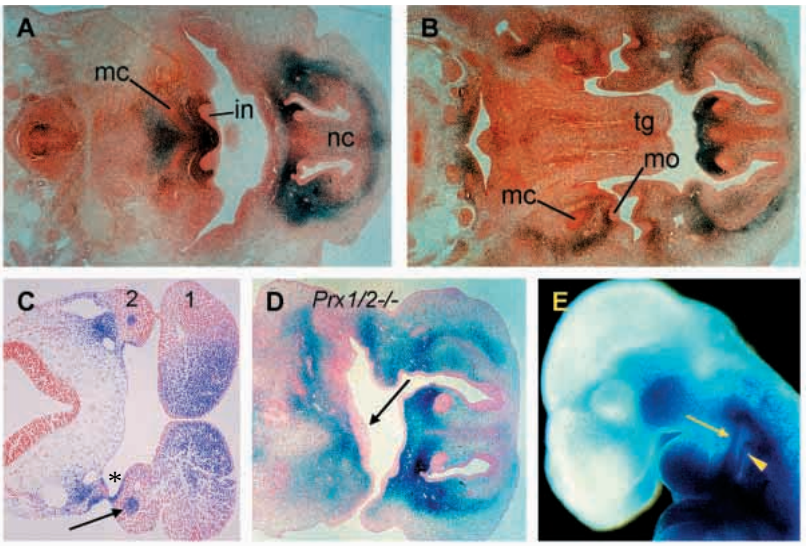

Fig. 6. Expression patterns of *Prx2* in pharyngeal arches and lower jaw as revealed by β-galactosidase activity in $Prx2^{+/-}$ and $Prx1^{-/-}Prx2^{-/-}$ mutant embryos. (A-C) Transverse sections of E12.5 (A,B), and E9.5 (C) $Prx2^{+/-}$ embryos. Arrow in C points to expression in the second pharyngeal arch, and asterisk indicates expression in the second pharyngeal pouch and cleft. (D) Transverse section through lower jaw of E12.5 $Prx1^{-/-}Prx2^{-/-}$ mutant embryo at level comparable to that of A. Arrow indicates abnormally thickened epithelium. (E) Whole mount of an E9.5 $Prx2^{+/-}$ embryo. Arrow indicates rod of *Prx2*-expressing mesenchyme in second arch and arrowhead indicates expression in second pharyngeal groove. Abbreviations: 1, mandibular component of first pharyngeal arch; 2, second pharyngeal arch; in, incisor bud; mc, condensation for Meckel's cartilage; mo, molar bud; nc, condensation for nasal cartilage; tg, tongue.

(Fig. 9C). A remnant of the lateral duct located in a small cavity in the otic capsule was apparent in sections of new-born animals (not shown). A slight reduction in the size of the otic capsule was found in $Prx1^{-/-}$ mutants (Fig. 9B).

The semicircular ducts develop from diverticula that grow out of the otocyst. The lateral wall of each diverticulum delaminates at its centre from the surrounding mesenchyme and coalesces with the opposite wall, forming the fusion plate. The fusion plate disintegrates and a semicircular duct remains. In wild-type embryos, all three semicircular ducts were formed at E12.5. In $Prx1^{-/-}Prx2^{-/-}$ embryos, the anterior diverticulum was much smaller than in wild-type controls, the lateral wall had delaminated from the surrounding mesenchyme, but fusion of the opposite walls had not yet occurred (compare Fig. 10A,C). The lateral diverticulum was present (Fig. 10D), but the posterior diverticulum was barely visible (Fig. 10C). At E13.5, the posterior diverticulum was a small outpocketing from the future common duct. The walls of the lateral duct had fused, although the duct was much smaller than in the control (data not shown). These observations indicate that the otic-capsule phenotype in $Prx1^{-/-}Prx2^{-/-}$ mutants is the result of reduced outgrowth of the ducts of the membranous labyrinth.

Prx2 expression is present in the lateral wall of the otocyst at E9.5 and E10.5 (Opstelten et al., 1991). Fate map studies have attributed this part to the future vestibule (Li et al., 1978). β-galactosidase staining of E11.5 and E12.5 $Prx2^{+/-}$ embryos showed expression in three domains of the developing otocyst: dorsoanteriorly on the diverticulum of the lateral duct, on the anterior side of the diverticulum of the posterior duct and on the anterior side of the anterior duct (Fig. 10F and data not shown). In addition, from E9.5 to E12.5 high expression was found in the mesenchyme surrounding the lateral side of the otocyst and around the outgrowing diverticula (Opstelten et al., 1991; shown for E11.5 in Fig. 10F). *Prx1* expression could not be detected in the otocyst from E9.5 to E12.5 using radioactive RNA in situ hybridisation (Fig. 10E and data not shown), but was high in the mesenchyme surrounding the lateral aspect of the otocyst and the diverticula of the developing ducts (Fig. 10E). Since outgrowth of the diverticula occurs in interaction with the surrounding mesenchyme (Swanson et al., 1990; Anniko and Schacht, 1984), these observations suggest that *Prx1* or *Prx2* activity in the mesenchyme is required for these interactions. The significance of *Prx2* expression in the otocyst remains unclear, as $Prx2^{-/-}$ mutants have no inner ear defects.

Skeletal abnormalities in other parts of the head and in the axial skeleton

In $Prx1^{-/-}$ and $Prx1^{-/-}Prx2^{-/-}$ mutants, the squamosal and the zygomatic bones were absent and the lateral wall of the skull was made up of a sheet of ectopic cartilage instead (Martin et al., 1995; Fig. 5C,E). The malar process of the maxillary bone was also absent in $Prx1^{-/-}Prx2^{-/-}$ mutants, so that the entire zygomatic arch was deleted (Fig. 5E). The palatal processes of

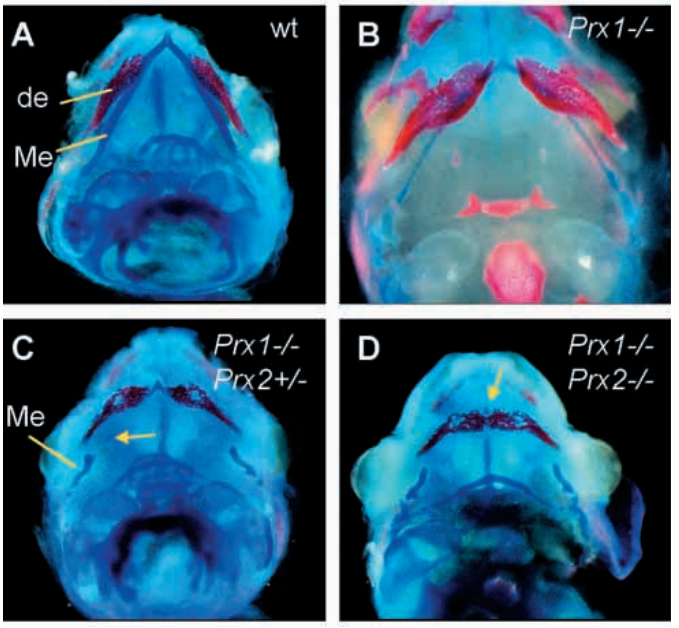

Fig. 7. Meckel's cartilage is truncated in E14.5 (C) $Prx1^{-/-}Prx2^{+/-}$ and (D) $Prx1^{-/-}Prx2^{-/-}$ mutant embryos. (A) Wild-type, (B) $Prx1^{-/-}$ embryo of a slightly more advanced stage than the others. (C) Arrow indicates fragment of Meckel's cartilage. (D) Note cartilaginous sphere at tip of jaw (arrow). Abbreviations: de, dentary bone; Me, Meckel's cartilage.

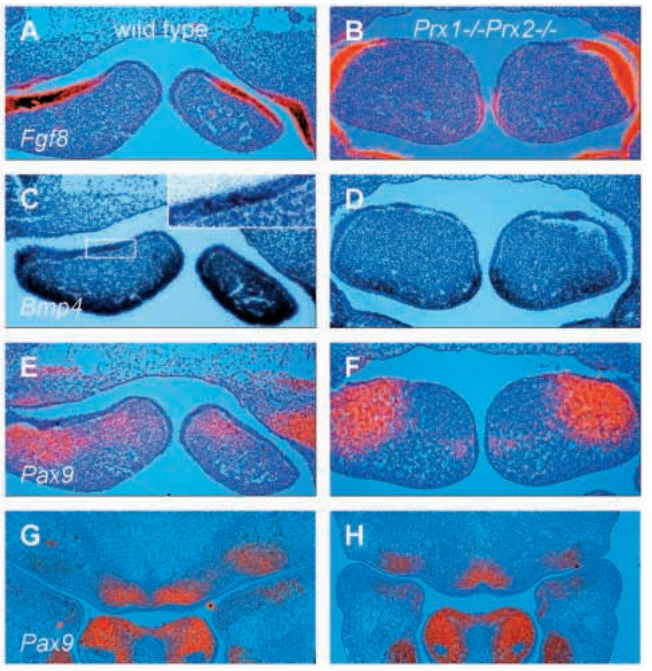

Fig. 8. Altered expression of *Bmp4*, *Fgf8* and *Pax9* in mandibular arch of *Prx1*$^{-/-}$*Prx2*$^{-/-}$ mutants. Transverse sections through mandibular arch of E11.0 (A-F) and E11.5 (G,H) wild-type (A,C,E,G) and *Prx1*$^{-/-}$*Prx2*$^{-/-}$ (B,D,F,H) embryos. Sections have been hybridised with probes for *Fgf8* (A,B), *Bmp4* (C,D) and *Pax9* (E-H). Inset in C is an enlargement of the boxed area, to indicate expression more clearly. Note that expression at corresponding position in D is absent. All except C,D are red-filtered dark-field images superimposed on a bright-field image. Dorsal is up.

the maxillae are hypoplastic in *Prx1*$^{-/-}$ mutants (Martin et al., 1995), but were completely absent in *Prx1*$^{-/-}$*Prx2*$^{-/-}$ mutants. An ectopic crescent-shaped cartilaginous element was located in the remnant of the auricle in *Prx1*$^{-/-}$*Prx2*$^{-/-}$ mutants (data not shown).

The dorsal processes of the thoracic and lumbar vertebrae are absent in *Prx1*$^{-/-}$ mutants, and the neural arches spread out laterally resulting in spina bifida (Martin et al., 1995). *Prx1*$^{-/-}$ *Prx2*$^{-/-}$ mutants showed in addition absence of the dorsal processes of the cervical vertebrae including the atlas and axis. While it has been reported that only 12% of *Prx1*$^{-/-}$ mutants show vertebral abnormalities (Martin et al., 1995), we found them in all *Prx1*$^{-/-}$ and *Prx1*$^{-/-}$*Prx2*$^{-/-}$ mutants examined (n=8 and n=26, respectively). In addition a hole was found in the xyphoid process of the sternum in *Prx1*$^{-/-}$*Prx2*$^{-/-}$ mutants (data not shown).

Abnormalities in the appendicular skeleton

Prx1$^{-/-}$ mutants show shortened zeugopods of forelimbs and hindlimbs and a slight bending of the preaxial elements (Martin et al., 1995; Fig. 11B,H). The zeugopods were much more shortened in *Prx1*$^{-/-}$*Prx2*$^{-/-}$ mutants, and the radius and tibia were strongly bent (Fig. 11D,E,I). The diaphysis of the tibia bulged out and formed a cap of bone under which the proximal and distal epiphyseal cartilages were connected (Fig. 11F,I). At E13.5, the cartilaginous precursors of the zeugopod bones were already shortened and thickened compared with wild type and, at E14.5, a bulge was visible on the radius and tibia, and ossification was delayed compared with wild type (not shown). This indicated that the phenotype was due to an early defect in formation of the skeletal precursors. However, longitudinal sections through the zeugopods of new-borns showed that, in the growth regions, the zones of prehypertrophic and hypertrophic cartilage cells were considerably shorter in *Prx1*$^{-/-}$*Prx2*$^{-/-}$ mutants than in controls (not shown), indicating a later defect in ossification of these bones.

The first digit of the forefoot of *Prx1*$^{-/-}$*Prx2*$^{-/-}$ mutants was broadened, and its phalanges were thinned centrally as if they had a propensity to bifurcate (Fig. 11D,E). An extra digit was found on the posterior side of the forefoot. The morphology of the ectopic digit ranged from only a fragment of a metacarpal (Fig. 11D), to a complete metacarpal and two phalanges (Fig. 11E; Table 1). The triangular, which articulates with the ulna and the carpal bones, was laterally truncated, and the pisiform bone was fused to the ulna. The metacarpal of the extra digit articulated with the triangular and the ulna. The extra digit was often thinner than the other digits (Fig. 11E). Abnormalities in the autopod were also visible in *Prx1*$^{-/-}$ and *Prx1*$^{-/-}$*Prx2*$^{+/-}$ mutants, where the base of the metacarpal of the fifth digit was broadened and formed an articulation with the triangular and ulna (Fig. 11B,C). It thus appeared that with progressive loss of *Prx* function, skeletal precursors of the fifth digit expanded and ultimately formed an additional digit. This expansion was variable between and within individuals, as differences between left and right autopods of the same individual were common.

In the hindfoot, an ectopic cartilaginous element was found between the first and second metatarsal in *Prx1*$^{-/-}$*Prx2*$^{-/-}$ mutants (Fig. 11I). The tarsal bones were fused, but the pattern of fusions varied. Fusions were found between two or more of the following elements: the second and third cuneiform bones, the naviculare, tibiale, talus, cuboid, calcaneum and the ectopic metatarsal element (Fig. 11F,I).

The pubic symphysis was not formed in *Prx1*$^{-/-}$*Prx2*$^{-/-}$ mutant new-borns, resulting in a gap between the pubic bones (not shown). In about 60% of *Prx1*$^{-/-}$*Prx2*$^{-/-}$ neonates (Table 1), we found that the spine of the scapula was partially or completely absent (Fig. 12). The extent of the defect was often different between left and right sides of the same animal, and was visible from E13.5 onwards. Scapular abnormalities were not found in *Prx1*$^{-/-}$*Prx2*$^{+/-}$ or *Prx1*$^{-/-}$ mutant animals.

Mutations in 5′ *Hoxd* or *Hoxa* genes can result in limb abnormalities like those found in the *Prx1*$^{-/-}$*Prx2*$^{-/-}$ mutants (see Rijli and Chambon, 1997), including similar zeugopod abnormalities and postaxial polydactyly. Expression patterns of *Hoxd11* and *Hoxd13* were, however, not changed in limbs of E10.5 and E11.5 *Prx1*$^{-/-}$*Prx2*$^{-/-}$ mutants, as determined by whole-mount in situ hybridisation (data not shown).

DISCUSSION

In this paper, we show that mice homozygous for a *Prx2* allele that lacks the homeodomain and the aristaless domain develop normally. In contrast, mice mutant for *Prx1* develop a series of skeletal abnormalities (Martin et al., 1995). We now show that mice mutant for both genes display a range of novel skeletal abnormalities, as well as a more severe manifestation of the *Prx1* mutant phenotype. Most of the abnormalities were found

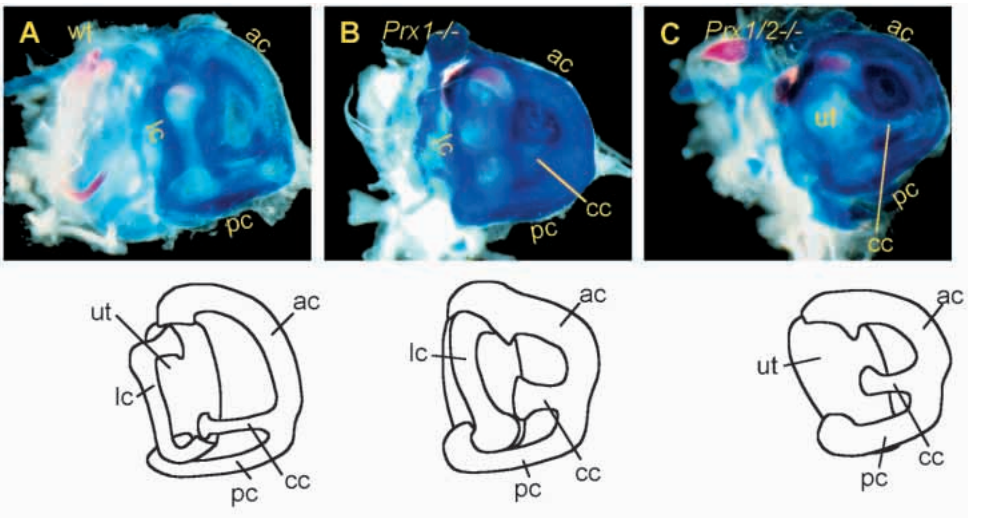

Fig. 9. Abnormal semicircular canals in *Prx1/2* mutant mice. Dissected otic capsules from wild-type new-born (A), $Prx1^{-/-}$ (B) and $Prx1^{-/-}Prx2^{-/-}$ mutant new-borns (C), with corresponding diagrams. Abbreviations: ac, anterior semicircular canal; cc, common canal; lc, lateral semicircular canal; pc, posterior semicircular canal.

in regions where both *Prx1* and *Prx2* are expressed (see Leussink et al., 1995, for a comparison of expression patterns). Although both *Prx1* and *Prx2* have been conserved in mammals as well as in birds (Leussink et al., 1995), the results indicate that *Prx1* can to a large extent substitute for *Prx2*.

Several aspects of the phenotype varied between individuals with the same combination of *Prx1* and *Prx2* alleles. Great variations were found in the phenotypes of the mandible, the shoulder girdle and the autopods of the limbs (Table 1). This is probably to a large extent a result of variation in genetic background of these animals, as they were offspring from individuals in which four different strains were represented. The presence of left-right differences in the limbs indicates that the source of variation is not only genetical, but that local stochastic variations may play a role as well.

Prx genes in skeletogenesis

Preskeletogenic condensations of many of the skeletal elements that were affected in the $Prx1^{-/-}Prx2^{-/-}$ mutants were abnormal. Therefore, *Prx1* and *Prx2* appear to regulate the formation of skeletal precursors. *Prx1* and *Prx2* are downregulated prior to or during condensation of the mesenchyme (Fig. 6B; Opstelten et al., 1991; Nohno et al., 1993; Kuratani et al., 1994; Leussink et al., 1995), and this suggests that they are required for early steps in the condensation process. As the defects are region specific, *Prx1* and *Prx2* may influence condensation in response to local positional cues.

In the bones of the zeugopods, we see that loss of *Prx1* and *Prx2* also has effect at a later stage of skeletogenesis, when the cartilaginous templates are replaced by bone. Ossification was delayed, the bones were shorter, and the growth regions were reduced in size, indicating a defect in proliferation or differentiation of cartilage. The radius was bent, suggesting that proliferation was less affected on the anterior side of this bone (see Fig. 11D). This side-specific effect was more extreme in the tibia, were ossification occurred on one side only (Fig. 11F,I). These results indicate that *Prx* genes do not only pattern embryonic precursors of the skeleton, but can also influence local growth rates in specific bones during foetal stages.

Prx1 and *Prx2* are not expressed in cartilage, but high expression has been reported in the perichondrium (Opstelten et al., 1991; Nohno et al., 1993; Kuratani et al, 1994; Leussink et al., 1995). The perichondrium has been shown to interact with signals from the growth region, and has a local effect on the rate of chondrocyte proliferation and differentiation (Vortkamp et al., 1996; Serra et al., 1997; Zou et al., 1997; Long and Linsenmayer, 1998). This suggests that the zeugopod phenotype is the result of abnormal functioning of the perichondrium in the $Prx1^{-/-}Prx2^{-/-}$ mutants. While the

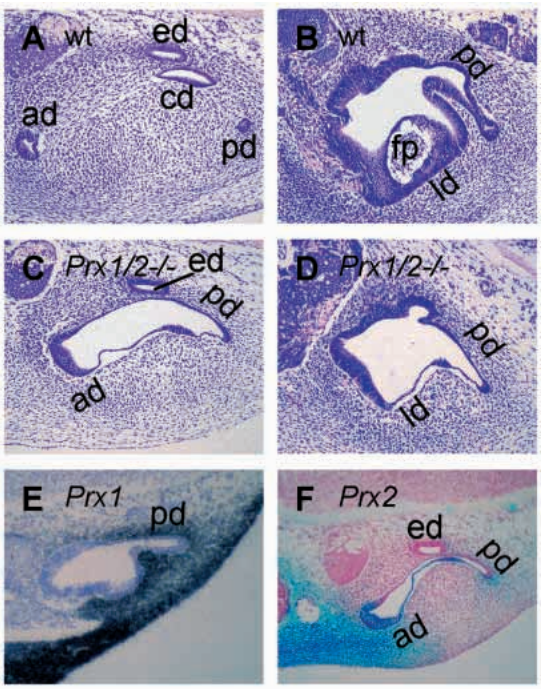

Fig. 10. Transverse sections through developing semicircular ducts in E12.5 wild-type (A,B) and $Prx1^{-/-}Prx2^{-/-}$ (C,D) embryos. Sections through anterior and posterior ducts (A,C) or lateral and posterior ducts (B,D). (E) Radioactive *Prx1* in situ hybridisation of transverse section through otic vesicle of E11.5 wild-type embryo. (F) *Prx2* expression in otic vesicle of E11.5 $Prx2^{+/-}$ embryo. Upper side is medial and right side is anterior. Abbreviations: ad, anterior semicircular duct; cd, common duct; ed, endolymphatic duct; fp, fusion plate; ld, lateral semicircular duct; pd, posterior semicircular duct.

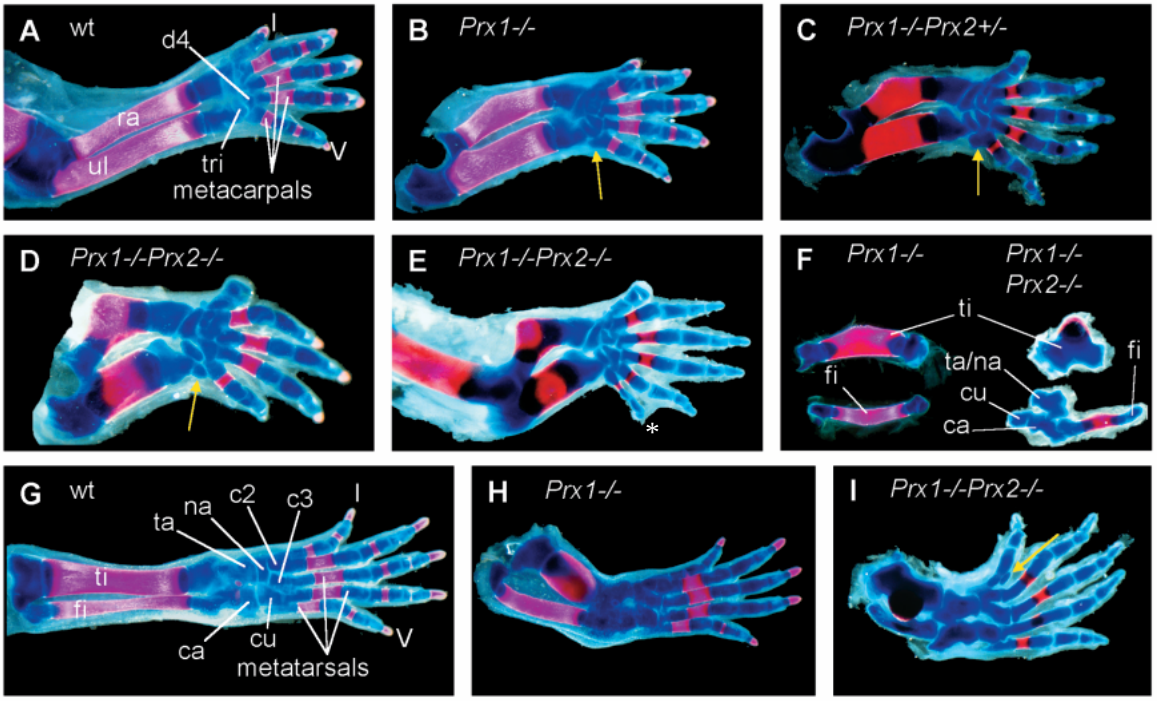

Fig. 11. Limb abnormalities in *Prx1/2* mutant mice. Skeletal preparations from right forelimbs (A-E) and hindlimbs (F-I) from wild-type (A,G), *Prx1*$^{-/-}$ (B,H), *Prx1*$^{-/-}$*Prx2*$^{+/-}$ (C), and *Prx1*$^{-/-}$*Prx2*$^{-/-}$ (D,E,I) new-borns. D is a mirror image of a left limb. (F) *Prx1*$^{-/-}$ (left) and *Prx1*$^{-/-}$*Prx2*$^{-/-}$ (right) mutant new-born hind limb zeugopods. The double mutant shows fusion of talus, naviculare, calcaneum, cuboid and fibula. (A-E) Upon progressive loss of *Prx1/2* function, the base of the fifth metacarpal expanded (arrow in B and C), formed the beginnings of a sixth metacarpal (arrow in D) and ultimately a new digit (asterisk in E). The triangular (tri) decreased concomitantly in size. The thumb (digit I) broadened upon loss of *Prx1/2* function (compare C-E with A), and radius and ulna were shorter and broader. Note the continuation between the radial epiphyseal cartilages in E. (G-I) Tibia and fibula shortened upon loss of *Prx1/2* function. In *Prx1*$^{-/-}$*Prx2*$^{-/-}$ mutants, the tibial diaphyseal ossification has shifted outwards (I). Yellow arrow in I points to ectopic metatarsal cartilage. The *Prx1*$^{-/-}$*Prx2*$^{-/-}$ mutant shown in I displays fusion of the talus and naviculare, and of the second and third cuneiform bones. Abbreviations: I-V, digits I-V; c2, second cuneiform bone; ca, calcaneum; cu, cuboid; d4, fourth distal carpal; fi, fibula; na, naviculare; ra, radius; ta, talus; ti, tibia; tri, triangular; ul, ulna.

mutant perichondrium showed normal morphology in sections (not shown), *Prx1* and *Prx2* may regulate components of signalling pathways in the perichondrium that influence chondrocyte proliferation or differentiation.

High expression of *Prx1* and *Prx2* is also found in the periosteum of several membrane bones, such as the dentary (not shown and Opstelten et al., 1991), maxillary, palatal process and malar process (data not shown). Since these bones are affected in the *Prx1*$^{-/-}$*Prx2*$^{-/-}$ mutant, it might be that the reduced outgrowth of these bones is a result of lack of *Prx1* and *Prx2* expression in the periosteum. These genes may then serve similar functions in the periosteum of membrane bones, as in the perichondrium of the zeugopod bones.

Prx genes in limb development

In addition to the zeugopod phenotype described above, *Prx1*$^{-/-}$*Prx2*$^{-/-}$ mutants showed postaxial polydactyly in the forelimb and a broadened thumb. This indicates an increased amount of mesenchyme in the hand plate, and suggests that *Prx1* and *Prx2* can influence rates of proliferation in the autopods or reduce cell death in the anterior and posterior necrotic zones. As both *Prx* genes are not expressed in the precartilaginous mesenchyme, they may function either in the mesenchyme surrounding the condensations, or earlier in the progress zone where they may pattern the limb during outgrowth.

Although mutations in 5′ *Hoxd* or *Hoxa* genes can result in limb abnormalities like those found in the *Prx1*$^{-/-}$*Prx2*$^{-/-}$ mutants (see Rijli and Chambon, 1997), we did not find abnormal *Hoxd11* or *Hoxd13* expression in *Prx1*$^{-/-}$*Prx2*$^{-/-}$ limb buds. It is possible that the *Prx* genes are downstream of the *Hoxd* genes, or that they regulate similar target genes involved in limb morphogenesis. These two possibilities can be distinguished by studying *Prx* expression in *Hoxd* mutants.

Mice mutant for the *Alx4* gene, which is closely related to the *Prx* genes, show preaxial polydactyly and a small ectopic zone of polarising activity (ZPA) anterior in the limb bud, as evidenced by expression of Fgf4 and Shh (Qu et al., 1997a). These authors propose a role for *Alx4* in repressing ZPA formation anterior in the limb bud, and suggest that the ectopic ZPA is small because *Alx4* may function together with related genes like *Prx1* and *Prx2* in a partially redundant manner. The *Prx1/2* mutant showed no abnormalities that are consistent with an anterior ZPA and a role for these genes in restricting the ZPA seems unlikely. The aristaless-related gene *Alx3* is a more plausible candidate to compensate for loss of *Alx4*, as its sequence is more related to *Alx4* and it is expressed anteriorly in the limb bud (Ten Berge et al., 1998).

Prx genes in pharyngeal arch development

Absence of *Prx1* and *Prx2* resulted in a shortened mandible,

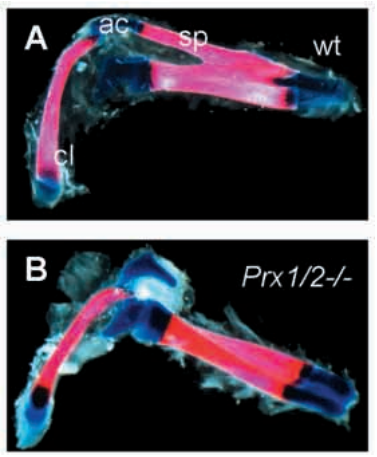

Fig. 12. Dissected scapula and clavicle from (A) a wild-type new-born and (B) a *Prx1*$^{-/-}$*Prx2*$^{-/-}$ mutant new-born. Abbreviations: ac, acromion process; cl, clavicle; sp, spine of scapula.

absence of a major part of Meckel's cartilage and reduction of the medial, incisor-containing, region to a degree that no or only a single incisor was present. During normal development, the lower jaw is formed from the mandibular component of the first pharyngeal arch. This is a bilaterally symmetrical structure, which initially consists of two processes that grow out from both sides of the future mouth cavity and fuse at their distal tips. These tips then form the medial area of the mandibular arch. *Prx1* and *Prx2* are both expressed in the mesenchyme of the distal tips (Fig. 6C; Nohno et al., 1993), and our results demonstrate that they are required for correct outgrowth of the lower jaw and for specification of the distal/medial compartment. The occurrence of mutants with cleft mandible indicates a failure of fusion of the processes. This may be explained by delayed outgrowth of the mandibular processes, which therefore could not meet within a time window in which the ectoderm is capable to fuse. Although the mandibular processes appeared morphologically normal prior to fusion, the cleft mandible phenotype had a low penetrance and the embryos studied may have been normal in this respect.

Neubüser et al. (1997) proposed a model in which antagonistic interactions between Bmp2/4 and Fgf8 in the mandibular arch epithelium determine the expression of *Pax9* in the underlying mesenchyme, which in turn would determine the position of the teeth. The *Prx1*$^{-/-}$*Prx2*$^{-/-}$ mutant exhibited changes in expression of *Bmp4* and *Fgf8* in the mandibular arch epithelium, and *Pax9* was expressed in the mesenchyme at the distal/medial tips of the arch, underneath an area of *Fgf8* expression. The distal/medial domain of *Pax9* correlates well with the position of the incisor in *Prx1*$^{-/-}$*Prx2*$^{-/-}$ mutants. The observation that, in a mutant context, the expression domains of *Bmp4*, *Fgf8* and *Pax9* change in such a way as to reliably predict the abnormal position of the incisor strongly supports the model of Neubüser et al. (1997). Ectopic *Fgf8* and *Pax9* expression was rather weak. This may explain the variability in the number of incisors as the result of a threshold situation in which small changes in *Fgf8* signal may result in loss or gain of an incisor.

The domain of ectopic *Pax9* expression is most likely the result of altered *Fgf8* expression, and not that of direct regulation by *Prx1/2*. Since both *Prx* genes are expressed in the mesenchyme but not in the epithelium, they cannot directly regulate *Fgf8*. The extended domain of expression of *Fgf8* may be an indirect consequence of distorted growth of the mandibular process, or the *Prx* genes may mediate interactions between the epithelium and the underlying mesenchyme that restrict *Fgf8* expression in the epithelium. Tissue recombination studies have demonstrated that the epithelium is required for outgrowth and correct skeletogenesis in the first arch (Hall, 1980), and this suggests a role for *Prx1* and *Prx2* in regulating epitheliomesenchymal interactions that promote outgrowth and skeletogenesis in the lower jaw.

Other members of the aristaless-related gene family in vertebrates include *Alx3*, *Alx4* and *Cart1*, and it is noteworthy that these genes are expressed in the distal part of the mandibular arch much like *Prx1* and *Prx2* (Ten Berge et al., 1998; Qu et al., 1997a,b; Zhao et al., 1994). Loss-of-function mutants have been generated for *Alx4* and *Cart1*, but neither show strong mandibular abnormalities (Qu et al., 1997a; Zhao et al., 1996). As in the case of *Prx1* and *Prx2*, redundancy of these genes may prevent a stronger phenotype of the mandible and combined mutants may prove insightful with respect to pharyngeal arch development.

The ectopic cartilage at the lateral wall of the skull of *Prx1*$^{-/-}$ mutants is essentially unchanged in *Prx1*$^{-/-}$*Prx2*$^{-/-}$ mutants. This cartilage has previously been interpreted as a manifestation of an atavistic quadrate cartilage (Martin et al., 1995). Based on anatomy and evolution of the first pharyngeal arch in mammals and their ancestors, however, Smith and Schneider (1998) argue that this ectopic cartilage cannot be homologous to the quadrate. Instead they propose that, since the dermal bones do not form, accumulation of excess undifferentiated mesenchymal cells may contribute to small pre-existing prechondrogenic condensations and cause them to exceed the minimum size limit required to undergo chondrification. A careful analysis of cell migration and condensation in this area is required to resolve this issue.

Prx genes in inner ear development

In *Prx1*$^{-/-}$*Prx2*$^{-/-}$ mutants, the formation of the diverticula of the future semicircular ducts was delayed and incomplete, but delamination and fusion of the walls of the diverticula occurred more or less normally. Experiments with otocyst explants cultured with and without periotic mesenchyme have shown that reciprocal interactions between otocyst and periotic mesenchyme are required for correct formation of the otic capsule. The periotic mesenchyme undergoes chondrification, but a signal from the developing ducts inhibits this in the mesenchyme surrounding the ducts (Frenz and Van De Water, 1991). As a consequence, the ducts lie in canals consisting of undifferentiated mesenchyme and surrounded by cartilage. As the lateral duct was strongly reduced in the *Prx1*$^{-/-}$*Prx2*$^{-/-}$ mutant, the circumference of the duct was probably so small that, instead of a lateral canal, a single cavity was formed in the otic capsule. According to this interpretation, absence of the lateral canal was a secondary consequence of retarded development of the membranous lateral duct.

Although *Prx2* showed a specific expression pattern in the diverticula of the otocyst, *Prx1* expression in the otocyst was not found, while both genes were highly expressed in the mesenchyme surrounding the diverticula. These results suggest that *Prx* activity is required in the surrounding mesenchyme

for correct outgrowth of the diverticula. Experiments with otocyst explants have provided evidence that the otocyst requires mesenchyme-derived signals for correct morphogenesis of the ducts (Swanson et al., 1990; Anniko and Schacht, 1984). We propose therefore that *Prx* genes are involved in epitheliomesenchymal interactions that promote outgrowth of the semicircular ducts.

We thank Rik Bleijs for isolating the *Prx2* cDNA clone, Arnold de Haan (Amsterdam) for measurements on the muscle/tendon complexes in *Prx2* mutants, Mohamed el Khatabbi for performing *Prx1* in situ hybridisation, Eric N. Olson (Dallas) for providing *Prx1* mutant mice, Sjef Verbeek (Utrecht) and Nathalie van der Lugt for help and advice on gene targeting, Els Robanus-Maandag and Anton Berns (Amsterdam) for IB10 ES cells, and Frank Oerlemans and Bé Wieringa (Nijmegen) for advice and SNLH9 feeder cells. Also thanks to Rudi Balling (Munich) for introducing one of us to aggregation techniques, and Jacqueline Deschamps for helpful comments on the manuscript. J. F. M. was supported by a grant from the NIDR (R29 DE12324-01).

REFERENCES

Anniko, M. and Schacht, J. (1984). Inductive tissue interactions during inner ear development. *Arch. Otorhinolaryngol.* **240**, 17-33.

Avé, P., Colucci-Guyon, E., Babinet, C. and Huerre, M. (1997). An improved method to detect β-galactosidase activity in transgenic mice: a post-staining procedure on paraffin embedded tissue sections. *Transgen. Res.* **6**, 37-40.

Cserjesi, P., Lilly, B., Bryson, L., Wang, Y., Sassoon, D. A. and Olson, E. N. (1992). MHox: a mesodermally restricted homeodomain protein that binds an essential site in the muscle creatine kinase enhancer. *Development* **115**, 1087-1101.

De Haan, A., Jones, D. A. and Sargeant, A. J. (1989). Changes in velocity of shortening, power output and relaxation rate during fatigue of rat medial gastrocnemius muscle. *Pflugers Arch.* **413**, 422-428.

De Jong, R. and Meijlink, F. (1993). The homeobox gene S8: mesoderm-specific expression in presomite embryos and in cells cultured *in vitro* and modulation in differentiating pluripotent cells. *Dev. Biol.* **157**, 133-146.

Erlebacher, A., Filvaroff, E. H., Gitelman, S. E. and Derynck, R. (1995). Toward a molecular understanding of skeletal development. *Cell* **80**, 371-378.

Frenz, D. A. and Van De Water, T. R. (1991). Epithelial control of periotic mesenchyme chondrogenesis. *Dev. Biol.* **144**, 38-46.

Hall, B. K. (1980). Tissue interactions and the initiation of osteogenesis and chondrogenesis in the neural crest-derived mandibular skeleton of the embryonic mouse as seen in isolated murine tissues and in recombinations of murine and avian tissues. *J. Embryol. Exp. Morph.* **58**, 251-264.

Hall, B. K. and Miyake, T. (1995). Divide, accumulate, differentiate: cell condensation in skeletal development revisited. *Int. J. Dev. Biol.* **39**, 881-893.

Hogan, B., Beddington, R., Costantini, F. and Lacy, E. (1994). *Manipulating the Mouse Embryo.* Second edition, New York: Cold Spring Harbor Laboratory Press.

Kern, M. J., Witte, D. P., Valerius, M. T., Aronow, B. J. and Potter, S. S. (1992). A novel murine homeobox gene isolated by a tissue specific PCR cloning strategy. *Nucleic Acids Res.* **20**, 5189-5195.

Kozak, M. (1987). An analysis of 5′-noncoding sequences from 699 vertebrate messenger RNAs. *Nucleic Acids Res.* **15**, 8125-8132.

Kuratani, S., Martin, J. F., Wawersik, S., Lilly, B., Eichele, G. and Olson, E. N. (1994). The expression pattern of the chick homeobox gene *gMHox* suggests a role in patterning of the limbs and face and in compartmentalization of somites. *Dev. Biol.* **161**, 357-369.

Leussink, B., Brouwer, A., El Khattabi, M., Poelmann, R. E., Gittenberger-de Groot, A. C. and Meijlink, F. (1995). Expression patterns of the paired-related homeobox genes *MHox/Prx1* and *S8/Prx2* suggest roles in development of the heart and the forebrain. *Mech. Dev.* **52**, 51-64.

Li, C. W., van de Water, T. R. and Ruben, R. J. (1978). The fate mapping of the eleventh and twelfth day mouse otocyst: an in vitro study of the sites of origin of the embryonic inner ear sensory structures. *J. Morphol.* **157**, 249-267.

Long, F. and Linsenmayer, T. F. (1998). Regulation of growth region cartilage proliferation and differentiation by perichondrium. *Development* **125**, 1067-1073.

Martin, J. F., Bradley, A. and Olson, E. N. (1995). The *paired*-like homeo box gene MHox is required for early events of skeletogenesis in multiple lineages. *Genes Dev.* **9**, 1237-1249.

Neubüser, A., Peters, H., Balling, R. and Martin, G.R. (1997). Antagonistic interactions between FGF and BMP signalling pathways: a mechanism for positioning the sites of tooth formation. *Cell* **90**, 247-255.

Nohno, T., Koyama, J. E., Myokai, F., Taniguchi, S., Ohuchi, H., Saito, T. and Noji, S. (1993). A chicken homeobox gene related to *Drosophila paired* is predominantly expressed in the developing limb. *Dev. Biol.* **158**, 254-264.

Opstelten, D. E., Vogels, R., Robert, B., Kalkhoven, E., Zwartkruis, F., de Laaf, L., Destrée, O. H., Deschamps, J., Lawson, K. A. and Meijlink, F. (1991). The mouse homeobox gene, *S8*, is expressed during embryogenesis predominantly in mesenchyme. *Mech. Dev.* **34**, 29-42.

Qu, S., Niswender, K.D., Ji, Q., van der Meer, R., Keeney, D., Magnuson, M.A. and Wisdom, R. (1997a). Polydactyly and ectopic ZPA formation in Alx-4 mutant mice. *Development* **124**, 3999-4008.

Qu, S., Li, L., Wisdom, R. (1997b). Alx-4: cDNA cloning and characterization of a novel paired-type homeodomain protein. *Gene* **203**, 217-223.

Rijli, F.M. and Chambon, P. (1997). Genetic interactions of *Hox* genes in limb development: learning from compound mutants. *Curr. Opin. Genet. Dev.* **7**, 481-487.

Rudnick, A., Ling, T.Y., Odagiri, H., Rutter, W.J. and German, M.S. (1994). Pancreatic beta cells express a diverse set of homeobox genes. *Proc. Natl. Acad. Sci. USA* **91**, 12203-12207.

Serra, R., Johnson, M., Filvaroff, E.H., LaBorde, J., Sheehan, D.M., Derynck, R. and Moses, H.L. (1997). Expression of a truncated, kinase-defective TGF-β type II receptor in mouse skeletal tissue promotes terminal chondrocyte differentiation and osteoarthritis. *J. Cell Biol.* **139**, 541-552.

Smith, K.K. and Schneider, R.A. (1998). Have gene knockouts caused evolutionary reversals in the mammalian first arch? *BioEssays* **20**, 245-255.

Swanson, G.J., Howard, M., Lewis, J. (1990). Epithelial autonomy in the development of the inner ear of a bird embryo. *Dev. Biol.* **137**, 243-257.

Te Riele, H., Robanus Maandag, E., Clarke, A., Hooper, M. and Berns, A. (1990). Consecutive inactivation of both alleles of the pim-1 proto-oncogene by homologous recombination in embryonic stem cells. *Nature* **348**, 649-651.

Ten Berge, D., Brouwer, A., El Bahi, S., Guénet, J., Robert, B. and Meijlink, F. (1998). Mouse *Alx3*: An *aristaless*-like homeobox gene expressed during embryogenesis in ectomesenchyme and lateral-plate mesoderm. *Dev. Biol.* **199**, 11-25.

Van Deursen, J. and Wieringa, B. (1992). Targeting of the creatine kinase M gene in embryonic stem cells using isogenic and nonisogenic vectors. *Nucleic Acids Res.* **20**, 3815-3820.

Vortkamp, A., Lee, K., Lanske, B., Segre, G.V., Kronenberg, H.M. and Tabin, C.J. (1996). Regulation of rate of cartilage differentiation by Indian Hedgehog and PTH-related protein. *Science* **273**, 613-621.

Wurst, W. and Joyner, A. L. (1993). Production of targeted embryonic stem cell clones. In *Gene Targeting*, The Practical Approach Series edn (ed. A. L. Joyner), pp. 33-61. Oxford: IRL Press.

Zhao, G.-Q., Zhou, X., Eberspaecher, H., Solursh, M. and deCrombrugghe, B. (1993). Cartilage homeoprotein 1, a homeoprotein selectively expressed in chondrocytes. *Proc. Natl. Acad. Sci. USA* **90**, 8633-8637.

Zhao, G., Eberspaecher, H., Seldin, M.F. and de Crombrugghe, B. (1994). The gene for the homeodomain-containing protein Cart-1 is expressed in cells that have a chondrogenic potential during embryonic development. *Mech. Dev.* **48**, 245-254.

Zhao, Q., Behringer, R.R. and de Crombrugghe, B. (1996). Prenatal folic acid treatment suppresses acrania and meroanencephaly in mice mutant for the Cart1 homeobox gene. *Nature genet.* **13**, 275-283.

Zou, H., Wieser, R., Massagué, J. and Niswander, L. (1997). Distinct roles of type I bone morphogenetic protein receptors in the formation and differentiation of cartilage. *Genes Dev.* **11**, 2191-2203.